Anal. Chem. **2002,** *74,* 3127−3133

Influence of Microstructure on the Electrochemical Performance of Tin-Doped Indium Oxide Film Electrodes

Natasha D. Popovich,* Sze-Shun Wong, and Brian K. H. Yen

Xanthon Inc., 104 T.W. Alexander Drive, Research Triangle Park, North Carolina 27709

Hyo-Young Yeom and David C. Paine

Division of Engineering, Brown University, Providence, Rhode Island 02912

The effect of the microstructure of tin-doped indium oxide (ITO) films on their electrochemical performance was studied using three redox probes, tris(2,2′-bipyridyl ruthenium(II) chloride ($Ru(bpy)_3^{2+/3+}$), ferrocyanide ($Fe(CN)_6^{4-/3-}$), and ferrocenemethanol ($FcCH_2OH^{0/+}$). ITO films were deposited using dc magnetron sputtering under a variety of conditions that resulted in films having different degrees of crystallinity, crystallographic texture, sheet resistance, surface roughness, and percent tin. It was found that the electron transfer for all three redox probes used in this study was more efficient at polycrystalline films than at amorphous ITO films. This effect is more pronounced at faster scan rates. The crystallographic texture of the ITO films, surface roughness, and a change in sheet resistance from 7.9 to 13.7 Ω/□ did not have an effect on electron-transfer kinetics. ITO films deposited using a 1 wt % SnO_2 target and having sheet resistance comparable to films deposited using a 10 wt % SnO_2 target had dramatically different microstructure from the films with higher weight percent Sn and were shown to perform poorly when used as electrode materials. We believe that the dramatic differences in electron-transfer kinetics observed at the various ITO films can be attributed to either the different density of defect sites along the grain boundaries or defect sites caused by substitutional Sn in the film.

Tin-doped indium oxide (ITO) thin films are used in a wide variety of optoelectronic devices that require optical transmissivity in the visible regime combined with reasonably low electrical resistivity ($(1-10) \times 10^{-4}$ Ω/□.[1,2] The unusually low resistivity of this wide-band gap semiconductor material is achieved by n-type doping to a degenerate state. The necessarily high n-type carrier concentration ($(5-10) \times 10^{19}$/cm^3) in ITO arises from two shallow donors: doubly charged oxygen vacancies and substitutional four-valent tin in the indium sublattice.[1]

Advances in application-specific processing methods for ITO played a critical role in the development of flat panel display technology.[3] ITO used in this application is typically deposited by dc magnetron sputtering[4,5] and has been optimized to achieve the highest possible optical transmissivity in the visible regime (∼90% at 550 nm) combined with the lowest possible resistivity. Process variables for the optimization of ITO are reviewed elsewhere[3] but include: substrate temperature (room temperature to 350 °C), postdeposition annealing conditions, composition of the ITO sputter target (0−10 wt % SnO_2), total Ar pressure (10−100 mTorr), oxygen content of the sputter gas (0−2 vol %), and sputter power. More recently, the interest in ITO films has intensified because of their use as anodes in organic light-emitting diodes (OLED),[6,7] which show great promise as a low-cost alternative to traditional LEDs and have been the subject of numerous studies. The use of ITO for electrochemical applications, where dramatically different properties are required compared to liquid crystal technology, has motivated this first report on the processing dependence of electrochemical performance of ITO.

Recently, there has been growing interest in the use of electrochemical methods for the analysis of biological molecules.[8,9] One particularly promising technology for the detection of nucleic acids is based on the electrochemical oxidation of guanine residues with a mediator, tris(2,2′-bipyridyl)ruthenium(II) ($Ru(bpy)_3^{2+}$).[10] The reaction between guanine and $Ru(bpy)_3^{2+}$ can be described by the two-step mechanism:

$$Ru(bpy)_3^{2+} \rightarrow Ru(bpy)_3^{3+} + e^- \quad (1)$$

$$Ru(bpy)_3^{3+} + \text{guanine} \rightarrow Ru(bpy)_3^{2+} + \text{guanine}_{ox} \quad (2)$$

The regenerated reduced mediator is again oxidized at the electrode, completing a catalytic cycle. The current produced

* To whom correspondence should be addressed. E-mail: npopovich@xanthon.com.

(1) Hamberg, I.; Granqvist, C. G. *J. Appl. Phys.* **1986**, *60*, R123−R159.
(2) Chopra, K. L.; Major, S.; Pandya, D. K. *Thin Solid Films* **1983**, *102*, 1−46.
(3) Lewis, B. G.; Paine, D. C. *MRS Bull.* **2000**, *25*, 22−28.
(4) Shigesato, Y.; Paine, D. C. *Thin Solid Films* **1994**, *238*, 44−50.
(5) Shigesato, Y.; Takaki, S.; Haranoh, T. *J. Appl. Phys.* **1992**, *71*, 3356−3364.
(6) Sheats, J. R.; Antoniadis, H.; Hueschen, M.; Leonard, J.; Miller, R.; Moon, R.; Roitman, D.; Stocking, A. *Science* **1996**, *273*, 884−888.
(7) Tang, C. W.; Van Slyke, S. A. *Appl. Phys. Lett.* **1987**, *51*, 913−918.
(8) Palecek, E., Fojta, M. *Anal. Chem.* **2001**, *73*, 75A−83A.

10.1021/ac011168l CCC: $22.00
Published on Web 05/09/2002

during each oxidation of $Ru(bpy)_3^{2+}$ is measured and reflects the amount of guanine present in the sample. In contrast to direct oxidation of guanine at an electrode, the electron-transfer reaction between $Ru(bpy)_3^{3+}$ and guanine is very fast (second-order rate constant was determined to be $\sim 1 \times 10^6$ M^{-1} s^{-1}).[11] The rapid electron transfer between $Ru(bpy)_3^{3+}$ and guanine has been primarily attributed to the nearly identical values for the standard reduction potential of guanine and $Ru(bpy)_3^{2+}$ (1.1 V vs SSCE).[12,13] Conducting ITO is the ideal electrode material for this application since it is stable at the high potentials required for guanine oxidation.[10,14] At these electrode potentials, the only viable nonoxide electrode alternatives are those based on graphitic carbon,[15] which was shown to be unsuitable in terms of both electron-transfer kinetics at the electrolyte/electrode interface and high nonspecific adsorption of nucleic acids.

Despite the wide range of potential applications of ITO in electrochemistry, very little is known about the factors that affect its electron-transfer properties. There are, for example, reports in the literature that appear to establish the importance of surface hydrophobicity/hydrophilicity[16] and surface treatments.[17] However, there is, to the best of our knowledge, very limited literature on the processing dependence of the performance of ITO electrodes used in electrochemistry. For example, Martinez et al.[18] studied the effect of sheet resistance on electrochemical performance of ITO films deposited by rf sputtering for two redox couples, $Fe(CN)_6^{4-/3-}$ and $Fe^{2+/3+}$, and found that low sheet resistance and high free carrier concentration of the film had a beneficial effect on electron transfer between the analyte and the electrode. The films with satisfactory performance were those obtained with postdeposition vacuum annealing treatments, but very limited film characterization was offered.

Numerous studies of electron-transfer kinetics on carbon surfaces have established the requirement for a high degree of heterogeneity of surface structure and properties.[19] For example, it has been shown that defects on highly ordered pyrolytic graphite (HOPG) are more reactive toward adsorption and electron transfer than the basal plane.[20,21] The slow electron-transfer kinetics at basal plane HOPG has been attributed to its low density of electronic states in the potential range of most redox systems, which is directly dependent on the variety of energy levels created by defects or functional groups. In the case of glassy carbon electrodes, electron-transfer rates are much faster due to the high disorder in the material resulting in a high density of electronic states.[20] Similar phenomena can be expected to be operational at ITO electrodes, since the nonstoichiometric nature of ITO leads to intrinsic heterogeneity of its surface.

In this work, we used dc magnetron sputtering to deposit ITO films under a range of conditions designed to establish the relationship between film microstructure, processing conditions, and electrochemical performance of ITO. Using conditions well within the process window for commercial ITO,[3] we have produced materials with similar resistivities but widely different crystallinity, film thickness, surface roughness, tin concentration, and crystallographic texture. These samples were used to establish the effect of process-dependent microstructure and doping on electrochemical performance. This work is the first step toward the design of an ITO microstructure that is optimized for electrochemical applications, with the ultimate goal of understanding the surface structural properties that control the electron-transfer reactivity of ITO electrodes.

EXPERIMENTAL SECTION

Indium tin oxide films were deposited onto Corning 7059 glass using dc magnetron sputter deposition in a dedicated high-vacuum system using commercial sintered In_2O-X wt % SnO_2 ($X = 1$ and 10) ceramic targets from Arconium Corp. The sputter target-to-substrate separation in this system was fixed at 10 cm, and the total gas pressure was fixed at either 10 or 100 mTorr. The system is turbopumped and prior to deposition the chamber pressure was reduced to 10^{-6} mTorr before being back-filled with ultrahigh pure Ar/O_2. It is well known that the resistivity of ITO depends on the ratio of O_2 to Ar during deposition and is optimized by finding the minimum in the u-shaped resistivity versus oxygen/argon ratio process curve.[22] The minimum resistivity is found at oxygen ratios that depend sensitively on process conditions (total pressure, Sn doping, sputter power, substrate temperature). For this reason, multiple samples were produced under a range of oxygen flows for each condition in order to establish the optimum resisitivity for each condition; in this work, we report only on the optimized films. This approach allowed us to compare samples with similar resistivities but different microstructural features. A set of six samples was deposited under conditions designed to establish the performance of amorphous versus crystalline and crystalline (400) versus (222) textured and the effect of film thickness (sheet resistance), root-mean-square (rms) surface roughness (1.6 versus 3.1 nm), and Sn concentration (1 versus 10 wt %).

The specific process conditions that were used for each of the six sets of samples discussed herein are summarized in Table 1. Details of the process dependence of ITO microstructure can be found elsewhere;[23] however, the essential process considerations are as follows. All samples are compared to our nominal standard process labeled II in Table 1. All samples were deposited to a thickness of 200 nm using a 10 wt % SnO_2 target except those in set V, where lower sheet resistance was produced by depositing a film ~400 nm thick, and set VI, where a 1 wt % SnO_2 target was used. Amorphous material (set I) was deposited using an unheated

(9) Anderson, J. L.; Coury, L. A., Jr.; Leddy, J. *Anal. Chem.* **2000**, *72*, 4497−4520.
(10) Johnston, D. H.; Glasgow, K. C.; Thorp, H. H. *J. Am. Chem. Soc.* **1995**, *117*, 8933−8938.
(11) Sistaire, M.; Holmberg, R.; Thorp H. H. *J. Phys. Chem.* **1999**, *103*, 10718−10728.
(12) Steenken, S.; Jovanovic, S. V. *J. Am. Chem. Soc.* **1997**, *119*, 617−619.
(13) Juris, A.; Balzani, V.; Barigelletti, F.; Campagna, S.; Belser, P.; von Zelewsky, A. *Coord. Chem. Rev.* **1988**, *84*, 85−277.
(14) Armstrong, N. R.; Lin, A. W. C.; Fujihira, M.; Kuwana, T. *Anal. Chem.* **1976**, *48*, 741−750.
(15) Szalai, V. A.; Thorp, H. H. *J. Phys. Chem. B.* **2000**, *104*, 6851−6859.
(16) Tominaga, M.; Kumagai, T.; Takita, S.; Taniguchi, I. *Chem. Lett.* **1993**, 1771−1774.
(17) Wu, C. C.; Wu, C. I.; Strum, J. C.; Kahn, A. *Appl. Phys. Lett.* **1997**, *70*, 1348−1350.
(18) Martinez, M. A.; Herrero, J.; Gutierez, M. T. *Electrochim. Acta* **1992**, *37*, 2565−2571.
(19) McCreery, R. L. In *Laboratory Techniques in Electroanalytical Chemistry*, 2nd ed.; Kissinger, P. T., Heineman, W. R., Eds.; Marcel Dekker: New York, 1996; Chapter 10.
(20) McDermott, M. T.; Kneten, K.; McCreery, R. L. *J. Phys. Chem.* **1992**, *96*, 3124.
(21) McDermott, M. T.; McCreery, R. L. *Langmuir* **1994**, *10*, 4307.
(22) Meng, Li.; dos Santos, M. P. *Appl. Surf. Sci.* **1997**, *120*, 243−249.
(23) Yeom, H.-Y.; Paine, D. C.; Wong, S.-S.; Popovich, N. D., manuscript in preparation.

Table 1. dc Magnetron Sputter Conditions for the Seven Samples Discussed in This Work

sample	substrate T (°C)	% O_2 in Ar	P_{total} (mTorr)	flow (sccm)	wt % SnO_2	sheet resistance (Ω/□)
(I) amorphous	RT	0.1	10	3	10	16.2 ±2.8
(II) standard	350	0.1	10	3	10	13.7 ±1.8
(III) texture (400)	350	0.1	10	7	10	14.7 ±1.7
(IV) roughness	350	0.1	100	3	10	14.2 ±2.3
(V) sheet resistance	350	0.1	10	3	10	7.9 ±0.7
(VI) Sn content	350	0.1	10	3	1	26.7 ± 5.3

substrate while all other substrates were heated to 350 °C during deposition. To control texture (set III), the total chamber pressure, substrate temperature, and gas composition were fixed and gas flow was increased (7 versus 3 sccm). In addition, the ITO surface roughness in this sputter system was observed to increase with total chamber pressure. Set IV was created using 100 mTorr total chamber pressure to increase the surface roughness (rms) from 1.6 nm at 10 mTorr to 3.1 nm at 100 mTorr.

The physical properties (resistivity, thickness, crystallography, surface roughness) of all films were characterized using standard techniques. Van der Paaw four contact resistivity measurements were made to determine sheet resistance, which was used together with thickness measured using X-ray reflectivity to determine the resistivity of the material. Crystallographic texture and crystallinity were determined using X-ray diffraction at a fixed incidence angle (3°) (GI-XRD) and parallel optics (Gobel mirrors). Tapping-mode atomic force microscopy (D3000, Digital Instruments) under ambient conditions was used to characterize the film surface roughness. Surface compositional analysis on the ITO electrodes was conducted using X-ray photoelectron spectroscopy (Physical Electronics Quantum 2000).

Electrochemical data with three common redox probes, tris-(2,2′-bipyridyl)ruthenium(II) chloride ($Ru(bpy)_3^{2+/3+}$), ferrocyanide ($Fe(CN)_6^{4-/3-}$) and ferrocenemethanol ($FcCH_2OH^{0/+}$), were obtained using a BAS-100W potentiostat (Bioanalytical Systems) with a single-compartment cell. Phosphate solution buffered to pH 7.0 was used as the supporting electrolyte. All chemicals were analytical reagent grade from Aldrich Sigma Chemical Co. and were used as received. The ITO working electrode area, defined by the size of an O-ring, was 0.28 cm^2. ITO electrodes were cleaned by sonication in deionized water, followed by sonication in 2-propanol and two more sonications in deionized water (15 min per sonication step). All potentials were measured and are reported with respect to a Ag/AgCl/3 M KCl reference electrode (Cypress Instruments). The counter electrode was a Pt wire (~1 cm^2). Deionized water, purified by passage through a Milli-Q Ultrapure water system (Millipore) filtration system, was used for all solution preparations. Electron-transfer rate constants were determined using the Nicholson method[24] ($D = 5 \times 10^{-6}$ cm^2/s, $\alpha = 0.5$).

RESULTS AND DISCUSSION

The amorphous samples (sample set I) were deposited at room temperature and a total chamber pressure of 10 mTorr with 0.1 vol % O_2 (see Table 1). This material was tested both as deposited and after annealing at 250 °C for 1 h (sample set Ia). The X-ray diffraction patterns taken from this material before (A) and after (B) annealing are presented in Figure 1 and clearly show a change with annealing from a single broad amorphous peak centered at $2\Theta = 30°$ to a set of sharp, well-defined peaks at positions expected for the primitive cubic lattice (80 atoms/unit cell) bixbyite crystal structure with a 1.01-nm lattice parameter.[25−27] The annealed films (sample set Ia) are clearly polycrystalline with roughly equal (222) and (400) intensity. The final sheet resistance of the amorphous and crystalline states was approximately the same at 16.2 ±2.8 versus 13.7 ±1.8 Ω/□, respectively. Optimization of the deposition process conditions, particularly oxygen content, was required to obtain amorphous and polycrystalline films with similar sheet resistance. The resistivity of ITO depends on both the carrier density and the carrier mobility. In ITO, carriers are provided by both oxygen vacancies and ionized Sn substitutionally positioned in In crystal sites. In the amorphous state, the number of carriers is small but their mobility is high due to the absence of ionized impurities and crystal defects such as grain boundaries. Upon crystallization, Sn becomes substitutional and ionized, which leads to an increase in carrier density, but the presence of now ionized impurities and grain boundaries decreases the mobility, offsetting the effect of an increase in carrier density.

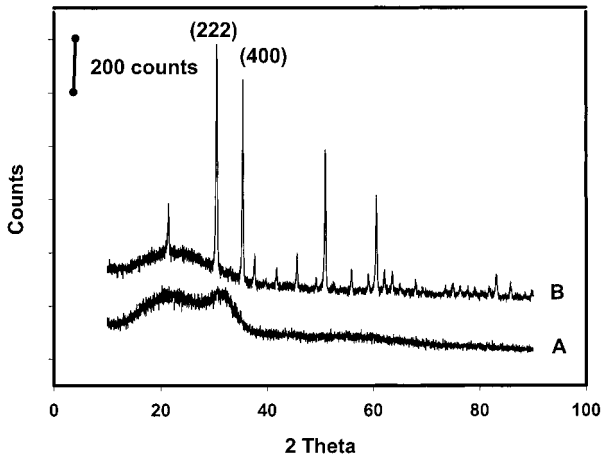

Figure 1. X-ray diffraction scans showing the room-temperature deposited film before (A) and after (B) annealing. Note the broad diffuse peak centered at $2\theta = 30°$ becomes a sharp, well-defined crystalline peak after annealing.

The electrochemical performance of the amorphous and crystallized films in electron-transfer reactions was assessed using

(24) Nicholson, R. *Anal. Chem.* **1965**, *37*, 1351−1355.

(25) Kerkache, L.; Sadaoui, K.; Layadi, A. *Eur. Phys. J. AP* **1998**, *1*, 177−180.
(26) Joshi, R. N.; Singh, V. P.; McClure, J. C. *Thin Solid Films* **1995**, *257*, 32−35.
(27) Martinez, M. A.; Herrero, J.; Gutierez, M. T. *Sol. Energy Mater. Sol. Cells* **1992**, *26*, 309−321.

Table 2. Kinetic Parameters for Three Redox Probes[a] at Amorphous and Polycrystalline ITO Electrodes

	ΔE_p (mV)		I_a (μA)		ET rate constant (cm/s)	
	as-deposited	annealed	as-deposited	annealed	as-deposited	annealed
$Rubpy^{2+/3+}$ 20 V/s	na[b]	146 ± 20	na	165 ± 5	na	0.030
$Rubpy^{2+/3+}$ 100 mV/s	154 ± 10	70 ± 5	5.5 ± 0.5	7.9 ± 1.0	0.0018	0.031
$Fe(CN)_6^{4-/3-}$ 100 mV/s	320 ± 20	162 ± 10	22 ± 2	28 ± 1	na	0.0015
$FcCH_2OH$ 100 mV/s	675 ± 25	227 ± 10	13.3 ± 0.5	20.4 ± 0.5	na	0.0015

[a] $Rubpy^{2+/3+}$: 100 μM $Ru(bpy)_3^{2+}$, 50 mM sodium phosphate buffered at pH 7.0. $Fe(CN)_6^{4-/3-}$: 500 μM ferrocyanide, 200 mM sodium phosphate buffered at pH 7.0. $FcCH_2OH$: 500 μM ferrocenemethanol 100 mM sodium phosphate buffered at pH 7.0. [b] na, signal not observed or rate constant too small to be calculated reliably.

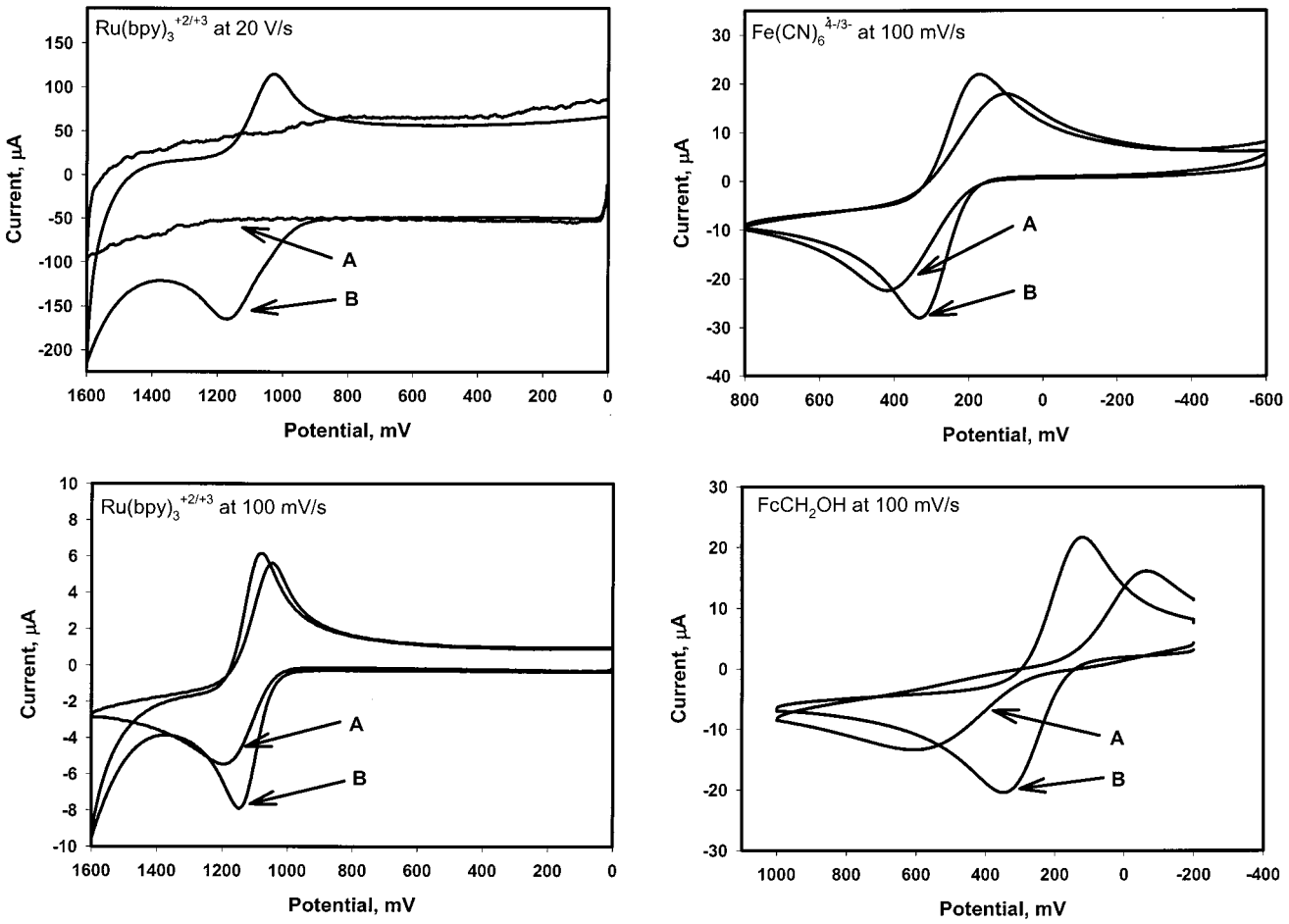

Figure 2. Cyclic voltammograms showing the electrochemical performance of amorphous (A) versus polycrystalline (B) ITO in electron-transfer reactions of three common redox probes, tris(2,2′-bipyridyl)ruthenium(II) ($Ru(bpy)_3^{2+}$), ferrocyanide ($Fe(CN)_6^{4-}$) and ferrocenemethanol ($FcCH_2OH$).

three common redox probes: tris(2,2′-bipyridyl)ruthenium(II) ($Ru(bpy)_3^{2+/3+}$), ferrocyanide ($Fe(CN)_6^{4-/3-}$), and ferrocenemethanol ($FcCH_2OH^{0/+}$). These analytes were chosen because of their charge differences and the fact that their electrochemical behavior at a variety of electrode materials is well documented and understood. For all of the differently charged redox probes, the electrochemical performance of the amorphous and polycrystalline ITO films followed the same trend. In the case of the amorphous material, electron-transfer rates for all examined probes were found to be considerably lower than those of the polycrystalline material, as evidenced by larger peak splitting and lower peak current (Table 2). The behavior of the amorphous (A) and crystalline (B) samples is compared in Figure 2 using cyclic voltammetry of the three redox probes. For example, the signal from $Ru(bpy)_3^{2+}$ cannot be observed at 20 V/s at amorphous ITO electrodes (A) but is apparent at the annealed ITO electrodes (B), suggesting more rapid electron-transfer kinetics after crystallization. As expected for a kinetic phenomenon, this effect is less pronounced at a slower scan rate ($Ru(bpy)_3^{2+}$ at 100 mV/s). The performance of ITO electrodes at fast scan rates was evaluated

because Armistead and Thorp[28] showed that the maximum catalytic current enhancement from the oxidation of surface-immobilized guanine is observed at scan rates of 10 V/s and higher. At slower scan rates, the catalytic current is more difficult to distinguish over the current due to the mediator alone. It is clear from these data that the amorphous ITO films are not a good electrode material for the mediated electrochemical oxidation of guanine, despite their low sheet resistance.

As shown in Figure 2, sluggish electron-transfer kinetics were observed for all three redox probes at the amorphous samples, despite their different redox potentials and charges. These data clearly demonstrate that changes in the microstructure of the ITO film are reflected in the electrochemical behavior of the film, with the polycrystalline state exhibiting more efficient electron transfer than the amorphous state. The ITO film allows for more efficient electron transfer in a polycrystalline versus amorphous state. We attribute this difference between polycrystalline and amorphous films to one of the following: (i) a greater density of defect sites along the grain boundaries that are active in electron transfer and that do not exist in the amorphous material or (ii) defect sites associated with substitutional tin in the crystalline bixbyite lattice that are not available in the amorphous state. Although the exact nature of the active electron-transfer sites is not known at this point, the higher density of defect sites along grain boundaries in ITO films is well documented and has been studied extensively for its role in determining the sheet resistance of ITO films.[29] Similarly, there is evidence in the literature[30,31] that Sn in the amorphous state is not electrically active. This is in contrast with polycrystalline material where Sn contributes to the high conductivity of the material.

To address the effect of the crystallographic texture on the electrochemical performance of ITO films, two sets of samples were produced at 350 °C, with optimized gas mixture conditions (0.1 vol % O_2 in Ar) and a total chamber pressure of 10 mTorr but at two different flow rates: 3 sccm for the standard samples (I) and 7 sccm for sample set III. The resulting change in crystallographic texture can be seen in Figure 3 and is consistent with increased (222) texture parallel to the sample surface. Note that the high flow rate produces films with a larger (400) peak (Figure 3, curve A) while the lower overall flow rate produced films in which the (222) peak dominates (Figure 3, curve B). The resistivity of these films was measured to be 14.7 ±1.7 and 13.7 ±1.8 Ω/□, respectively. Analysis of the cyclic voltammograms from these electrodes revealed no significant differences in electron-transfer rate associated with crystallographic texture.

The performance of ITO used in electrochemical applications is primarily determined by electron-transfer kinetics. Since the process of electron transfer is confined to the interface between the electrode and the electrolyte, the redox kinetics will be influenced by the effective surface area and density of active electron-transfer sites. To evaluate the effect of surface roughness on the rate of electron transfer, samples with two levels of surface roughness were produced by depositing ITO at standard (sample set II) and elevated (sample set IV) chamber pressures (10 vs

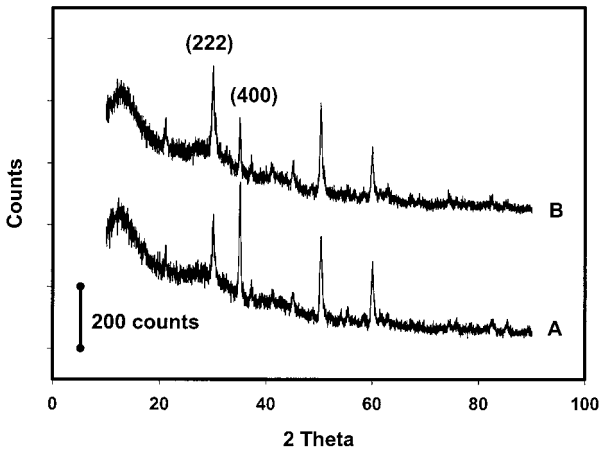

Figure 3. X-ray diffraction scans showing (A) 400 and (B) 222 dominant diffraction patterns. These films are fully crystalline and were deposited at 350 °C but with two different gas flow rates.

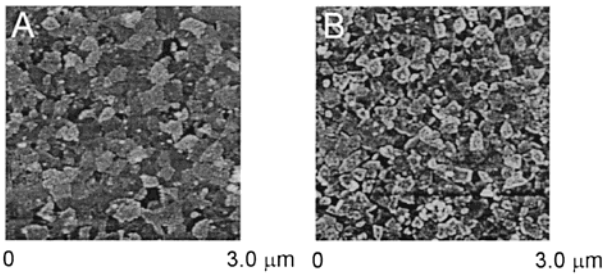

Figure 4. Atomic force microscopy images showing the surface of ITO deposited under (A) low (10 mTorr) and (B) high (100 mTorr) chamber pressure. R_{rms} values were 1.6 and 3.1 nm, respectively.

100 mTorr, respectively). Higher pressures have the effect of thermallizing the ions incident on the surface, which results in greater surface roughness. This is shown in the AFM images presented in Figure 4. From these AFM images, the rms surface roughness (3 × 3 μm scan size) was found to be 1.6 and 3.1 nm at low (A) and high (B) chamber pressures, respectively. Resistivity measurements of the ITO produced at the higher chamber pressure, with optimized oxygen flow, gave values of 14.2 ±2.3 Ω/□, which is comparable to the standard sample and most other samples reported in this work (see Table 1). The effect of roughness on the electron-transfer kinetics of $Ru(bpy)_3^{2+}$ is shown in Figure 5. The CVs show an increase in charging current with the use of increased chamber pressure during film deposition while no significant difference was recorded in the peak separation and peak current (with background correction).

The effect of ITO film sheet resistance on electrochemical performance was examined by voltammetry. The effect of a change in the series resistance on the electrochemical circuit was evaluated by increasing the total film thickness (sample set V). Early experiments demonstrated that a sheet resistance above ~100 Ω/□ renders the electrochemical signal undetectable over the background charging current, even when a slow scan rate (100 mV/s) is used to negate possible contributions from resistive/capacitive time constants. Sample set V was produced at twice the thickness of the standard materials (sample set II) but under otherwise identical conditions to produce a sample that had similar resistivity but half the sheet resistance (13.7 versus 7.9 Ω/□). The voltammograms of $Ru(bpy)_3^{2+}$ at the two materials (thin and

(28) Armistead, P. M.; Thorp, H. H. *Anal. Chem.* **2000**, *72*, 3764−3770.
(29) Kulkarni, A. K.; Schulz, K. H.; Lim, T. S.; Khan, M. *Thin Solid Films* **1999**, *345*, 273−277.
(30) Shigesato, Y.; Paine, D. C *Applied Phys. Lett.* **1993**, *62*, 1268−1270.
(31) Yi, C. H.; Yasui, I.; Shigesato, Y. *Jpn. J. Appl. Phys.* **1995**, *34*, 600−605.

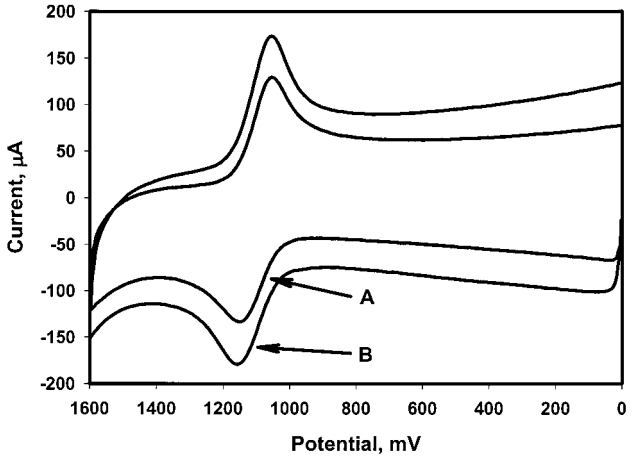

Figure 5. Cyclic voltammograms of $Ru(bpy)_3^{2+}$ at 20 V/s at standard, low-pressure, low-surface-roughness ITO, produced at 10 mTorr (A) and higher surface roughness ITO produced at 100 mTorr (B).

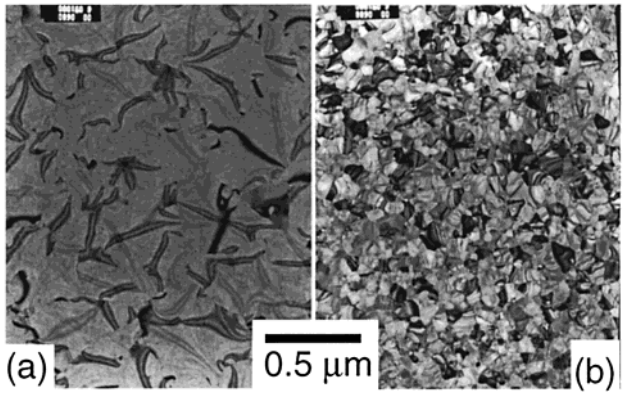

Figure 6. Plan view bright-field TEM images of (a) the 1 wt % SnO_2 sample and (b) the 10 wt % SnO_2 sample. Note the larger grain size (0.5 vs 0.05 μm) associated with the low tin sample.

thick) were indistinguishable, indicating that relatively small differences in the sheet resistance of ITO films have no effect on their electrochemical performance.

Finally, indium oxide is rendered degenerate by the presence of carriers donated by doubly charged oxygen vacancies and by ionized four-valent tin substituted in In sites. In this work, the role of Sn in electron transfer at the electrode/electrolyte interface was examined by creating two sets of samples from sputter targets having two different SnO_2 concentrations (1 and 10 wt %). The process conditions correspond to the standard conditions (sample set II) and Ar/O_2 ratios optimized for the low-Sn samples (sample set VI). Films deposited using 1% SnO_2 target had dramatically different microstructure from samples deposited with 10% SnO_2 target. Figure 6) shows bright-field TEM images of (a) the 1 wt % SnO_2 sample with a grain size of ~0.5 μm and (b) the 10 wt % sample with a grain size of ~0.05 μm. Indium-to-tin ratios obtained from XPS are 8 and 99 for the ITO prepared from 10 and 1 wt % SnO_2 sputter targets, respectively. As shown in Figure 7, cyclic voltammograms of $Ru(bpy)_3^{2+}$ obtained at sample sets II and VI with similar sheet resistance reveal that the 1% Sn samples (A) showed very sluggish electron transfer at a fast scan rate (20 V/s) when compared to 10% Sn samples (B). Similar data (not shown) were obtained using a slow scan rate (100 mV/s).

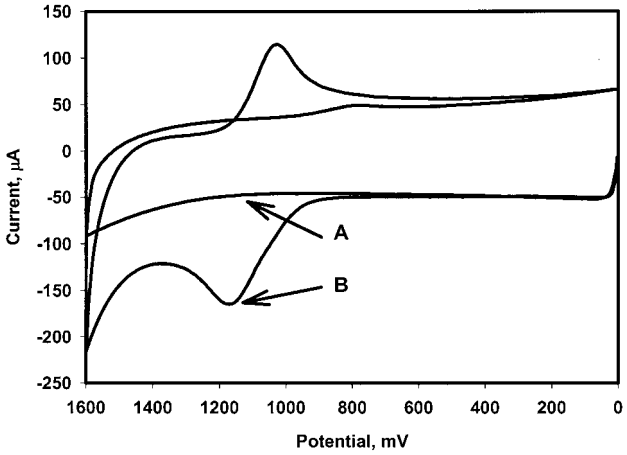

Figure 7. Cyclic voltammogram of $Ru(bpy)_3^{2+}$ at optimized films fabricated using (A) the 1 wt % SnO_2 ITO target and (B) the standard 10 wt % SnO_2. Scan rate, 20 V/s.

The observed difference in the behavior of sample sets II and VI can also be attributed to a difference in the density of defect sites along the grain boundaries, presumably the sites where electron transfer occurs, or to the effect of ionized Sn defect sites at the surface. Samples with lower Sn concentration have larger grains, and therefore a lower grain boundary/grain ratio. Quaas and Wullf studied films with different amount of Sn using GI-XRD and found that an increase in Sn concentration in ITO films causes an increase in lattice defects, as grain boundaries and microstrains.[32] This observation supports our findings and the importance of Sn in creating defect sites for electron-transfer events. The role of Sn in defining sites for electron-transfer events remains unclear, but our data show that electron transfer is sluggish in amorphous material where there are no grain boundaries and Sn reportedly does not provide carriers. Furthermore, in samples with low tin, where the grain size is considerably larger and the concentration of tin is necessarily low, electron transfer is again sluggish.

CONCLUSIONS

It is well known that the physical properties of ITO films depend greatly on the method and conditions of deposition.[3] These properties can be altered by postdeposition treatments, such as annealing. The work presented here demonstrates the dramatic effect that changes in the microstructure of ITO films have on their electrochemical performance. We have found that polycrystalline ITO films allow for more efficient electron transfer than amorphous films, while the crystallographic orientation in a polycrystalline film had no effect on its electron-transfer characteristics. This work also showed that high Sn concentration in the film is required, as it results in films with smaller grain sizes and more electron-transfer active sites. The nature of the active electron-transfer sites in ITO films is unknown, but it is clear from the data presented here that defect sites, either along grain boundaries or formed by substitutional Sn, play a major role in electron-transfer events. The insights gained in this work provide a deeper understanding of the relationship between processing and electrochemical performance of ITO films with the goal to

(32) Quaas, M.; Wulff, H. *Fresenius J. Anal. Chem.* **1998**, *361*, 617−618.

design ITO processing and postgrowth treatments that will result in optimal performance of ITO electrodes tailored for specific electrochemical applications.

ACKNOWLEDGMENT

The authors acknowledge helpful discussions with Profs. Dennis C. Johnson, Ed Bowden, and Neal Armstrong and partial support at Brown University from NSF through MRSEC DMR-0079964. The authors also thank Prof. Holden H. Thorp and Dr. David Stewart for their critical reading of the manuscript.

Received for review November 9, 2001. Accepted March 25, 2002.

AC011168L